Estimation of Aircraft Orientation From Flight Paths Using a Coordinated Flight Model

Lisa M. Ehrman and Aaron D. Lanterman

The authors are with the School of Electrical and Computer Engineering, Georgia Institute of Technology, Mail Code 0250, Atlanta, GA 30332 (e-mail: {lanterma,ehrman}@ece.gatech.edu).

Abstract

This paper presents an algorithm for computing probable orientation angles of an aircraft with a known flight path. The algorithm is derived from geometry and classical Newtonian physics. It is tested with a series of simulated flight paths that are selected to demonstrate algorithm performance under a variety of conditions, as well as with a real flight path collected from an instrumented F-15C. The algorithm generally performs well, but has some difficulty estimating aircraft roll.

I. Introduction

Most target tracking systems estimate positions and velocities from sensors such as radar, sonar, and infrared focal plane array. Various tracking filters associated with estimating these states are well understood. The orientation of the target, on the other hand, is often not observed by the sensors. The level of maneuverability of many aircraft makes it impossible to compute the exact orientation as a function of the flight path; hence, we present an algorithm for computing the most likely aircraft orientation based on position and velocity measurements.

Orientation information is helpful in adding automatic target recognition (ATR) capabilities to target tracking systems. Targets will take on different appearances depending on their orientation relative to the sensors. If the orientation of the target is included as a parameter which needs to be estimated, Newton's equations of motion couple the orientation and position estimates, suggesting that tracking and target recognition should be considered jointly. Accurate tracking assists in recognition, and similarly, accurate recognition and orientation estimation can assist in tracking. For instance, in a series of papers, Sworder and colleagues [1], [2], [3], [4], [5] discuss "image-enhanced" filters which augment low-resolution tracking information with visual imagery which helps the tracker know about maneuver changes. Kendrick, Maybeck, and Reid [6] assume that aircraft orientation is available from an imaging sensor and use that data to assist the tracker. Lefas [7] takes a similar approach, except he assumes that the aircraft are cooperatively transmitting orientation information provided by instruments on board the aircraft to the tracker. Miller, Srivastava, and Grenander [8] consider joint tracking and recognition using narrowband sensor array data together with high-resolution range profiles. In their approach, the Euler angles of the multiple aircraft are explicitly estimated. Their

algorithm samples from the resulting complicated Bayesian posterior distribution by simulating jump-diffusion processes [9]. A more sophisticated version by Srivastava *et al.* involving stochastic differential equations operating on Lie groups is given in [10], [11]. Herman [12], [13] has developed a similar approach to joint tracking and recogition with based on particle filters, with specific application to passive radar systems that exploit "illuminators of opportunity" such as FM radio and television broadcasts [14].

Both the jump-diffusion and particle filtering algorithms mentioned above are computationally intensive. This paper presents a simpler approach, where we take the position and velocity measurements to be "true," and estimate a likely orientation from those measurements based on a coordinated flight model. Our motivating application is ATR from passive radar data by comparing the RCS measured by various transmitter-target-receiver links with RCS predictions derived from a target RCS library which has been computed off-line. Ideally, the prediction would be made from simulated the various candidate target types at the same position and orientation as the true unidentified target.

A. Coordinate Conventions

The orientation angles that will be computed by the algorithm are aircraft yaw, heading, pitch, and roll. The conventions used for yaw, pitch, and roll are depicted in Figure 1.

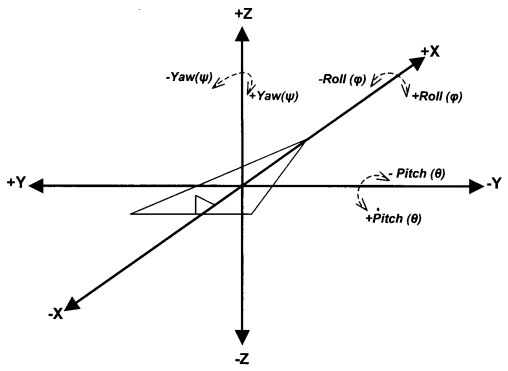

Fig. 1. Coordinate Convention Used to Compute Aircraft Yaw, Pitch, and Roll

The convention used in the computation of aircraft heading is shown in Figure 2. This complies with typical navigational conventions.

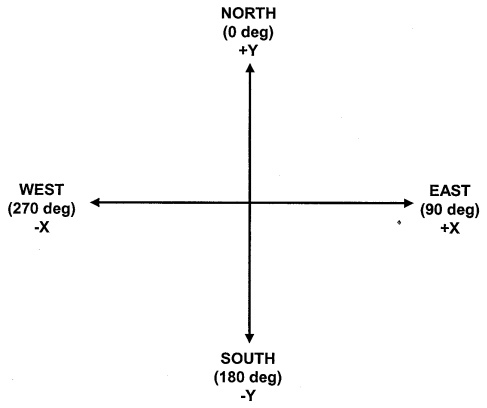

Fig. 2. Navigational Coordinate System Used to Compute Aircraft Heading

II. Computation of Yaw, Heading, and Pitch

A. Aircraft Yaw

As shown in Figure 1, the yaw of an aircraft describes the angular difference in the x-y plane between the aircraft's velocity vector and the direction of the aircraft nose. Conditions such as high wind and severe weather sometimes induce yaw in aircraft flight; however, under normal circumstances, the yaw for fixed-wing aircraft is approximately zero. For this reason, this paper assumes that yaw is always zero.

B. Aircraft Heading

Aircraft heading describes the association of cardinal directions with aircraft motion in the x-y plane. The convention adopted by this paper is shown in Figure 2, and is consistent with standard navigational practices. Since heading is a function of aircraft motion in the x-y plane, it can be written as a function of the x and y components of aircraft velocity. The equation for aircraft heading is given by

$$\xi = \begin{cases} 90 - \arctan(\frac{v_Y}{v_X}), x > 0 \\ 270 - \arctan(\frac{v_Y}{v_X}), x < 0 \end{cases} . \quad (1)$$

Since the equation provides a linear approximation, it is most accurate when the time between aircraft position samples is small.

C. Aircraft Pitch

The pitch of an aircraft describes the angle between the total velocity vector and the velocity vector in the x-y plane, and can be thought of as the angle at which the aircraft is changing altitude. Let (dx, dy, dz) denote the difference in aircraft position over a period of time, dt. The pitch is then given by

$$\theta = \arctan\left(\frac{dz}{\sqrt{dx^2 + dy^2}}\right). \tag{2}$$

Although this is a linear approximation, it should provide sufficient accuracy as long as the sampling rate of aircraft position is fairly high.

III. Computation of Aircraft Roll

Figure 1 depicts aircraft roll as the rotation of the aircraft about the vector that comes out of the aircraft nose in the direction of aircraft motion. This rotation can be performed by many high-performance aircraft without any deviation in the flight path or velocity, rendering it impossible to compute the roll angle as a function of flight path with a high degree of certainty. Even so, this paper is concerned with computing probable orientation angles, based upon a flight path. With that in mind, non-zero roll angles are considered to be the likeliest orientation only when the aircraft is executing a turn. In all other circumstances, the roll is assumed to be zero.

A. Constant-Altitude Turn

One of the simplest maneuvers in which an aircraft could be expected to roll is a constant-altitude turn [15] of radius R. A free body diagram of an aircraft executing such a turn is shown in Figure 3.

Since the aircraft is in equilibrium when executing the turn, the sum of the forces in the y-direction is equal to zero. From Figure 3 it is clear that the forces acting in the y-direction are the centrifugal force, F_C, and the y-component of the aircraft lift, L_Y. Thus, it is possible to write

$$L_Y = F_C. \tag{3}$$

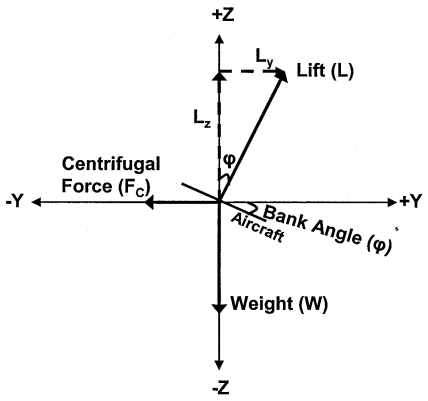

Fig. 3. Free Body Diagram of an Aircraft Executing a Constant-Altitude Banked Turn

The centrifugal force is derived from Newton's Second Law, in which $\frac{W}{g}$ is substituted for mass and $\frac{|v|^2}{R}$ is substituted for acceleration. Here W is the weight and g is the gravitational constant. The y-component of lift is related to the total lift through a simple trigonometric relation. Substitution of these expressions into (3) results in

$$L\sin(\phi) = \frac{W|v|^2}{Rg}. \tag{4}$$

Solving (4) for the roll angle yields

$$\phi = \arcsin\left(\frac{W|v|^2}{LRg}\right). \tag{5}$$

Since the aircraft is maintaining a constant altitude, the sum of the forces in the z-direction is also equal to zero. Figure 3) demonstrates that the forces acting in the z-direction are the weight, W, and the z-component of the lift, L_Z. Thus,

$$L_Z = W, \tag{6}$$

describes the equilibrium of forces in the z-direction. L_Z can be written as a function of total lift, L, and bank angle. This relation is substituted into (6), resulting in

$$L\cos(\phi) = W, \tag{7}$$

which can be solved for the bank angle, giving

$$\phi = \arccos\left(\frac{W}{L}\right). \tag{8}$$

Both weight and lift vary with aircraft type, which is unknown [16]. For this reason, it would be advantageous to derive an equation for the roll angle that is independent of weight and lift. Fortunately, this can be accomplished by combining (5) and (8) to give

$$\phi = \arctan\left(\frac{|v|^2}{Rg}\right). \tag{9}$$

The aircraft velocity can be easily derived from the aircraft flight path, and the force of gravity is a known constant. Thus, the only remaining unknown in (9) is the radius of the turn.

Computing the radius of turn would be relatively simple if aircraft always flew in perfect circles and began the turns instantaneously. However, this is not the case. Even if an aircraft were able to instantaneously snap into banked turns, the instantaneous G-loading induced by such maneuvers could be harmful for pilots. For this reason, it is common practice for aircraft to gradually transition into banked turns.

This gradual transition can be thought of as moving from a turn with a radius of curvature approaching infinity to a turn with a particular finite radius. Similarly, the transition out of a banked turn can be treated as moving from a turn with a finite radius to one with a radius approaching infinity. Thus, the transition made by an aircraft into or out of a banked turn is essentially just a curve with a uniformly changing degree of curvature. This type of curve is known as a spiral curve.

The radius of curvature at any point along a spiral curve can be found using the method of osculating circles. In this method, a "circular arc drawn tangent to the spiral at point P has a radius r equal to the radius of curvature of the spiral at the point of tangency" [17]. The circular arc is known as an osculating circle, whose radius of curvature is given by

$$R_{XY}(t) = \frac{[\dot{x}(t)^2 + \dot{y}(t)^2]^{3/2}}{\dot{x}(t)\ddot{y}(t) - \ddot{x}(t)\dot{y}(t)}, \tag{10}$$

where $x(t)$ and $y(t)$ are the x and y positions as functions of time. Using this method, the radius of curvature can be found for every position in the flight path. The resulting radius function can be substituted into (9) to compute roll as a function of time.

The sign of the roll angle must also be considered. Because the expression for roll given by (9) is a function of the magnitude of the velocity, the radius of acceleration, and the

pull of gravity, it always results in a positive roll angle. From Figure 1, it is clear that positive roll angles are associated with rolls in which the aircraft's right wing is down. If the aircraft is flying in a clockwise manner, then the roll angle should be positive, given the current convention. Conversely, counter-clockwise flight should result in negative roll angles.

A simple way to implement this convention is to test for counter-clockwise flight, and invert the sign of the roll angle when it is detected. A logical test for counter-clockwise flight in a certain incremental period of time, dt, is given by

$$[(dx < 0) \text{ and } (\text{CU})] \text{ or } [(\text{dx} > 0) \text{ and } (\text{CD})], \tag{11}$$

where CU denotes a flight path that is concave-up during dt, CD denotes a flight path that is concave-down during dt, and dx is the incremental distance traversed by the aircraft in the x-direction during dt. Applying this test to the values computed with (9) results in the computation of aircraft roll in accordance with the conventions selected in Figure 1.

B. General Case

Section III-A describes a method for computing aircraft roll as a function of time, given nothing but a time-correlated flight path; however, since it hinges on the assumption that the sum of forces in the z-direction is equal to zero, it only applies when the aircraft maintains a constant altitude. This methodology must, then, be expanded to account for the possibility that the aircraft changes altitude as it maneuvers.

Equations 3 through 5 provide a method for computing roll angles that is not dependent upon maintaining a constant altitude. However, the equations are dependent upon aircraft weight and lift, parameters which vary from one aircraft to another. Since aircraft type is not known, a method for computing the roll angle that is not dependent upon aircraft weight and lift is desirable.

One solution to this dilemma is to select a coordinate system in which the aircraft is not changing altitude. This is accomplished by first rotating the x-y plane such that all of the motion in the new x'-y' plane occurs in the +x'-direction. If this is followed by a rotation of the x'-z plane, then all of the aircraft motion in the newly-created x"-y'-z' space will be parallel to the x"-axis. Note that this process must be repeated at every time increment

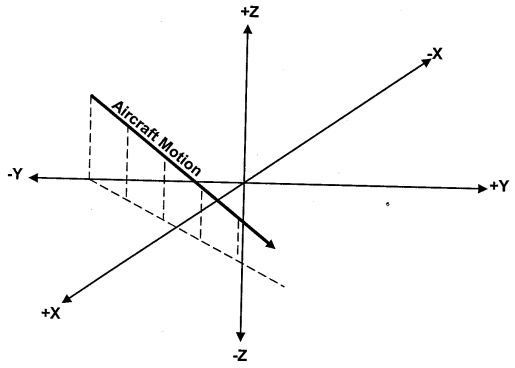

Fig. 4. Aircraft Motion in x-y-z space

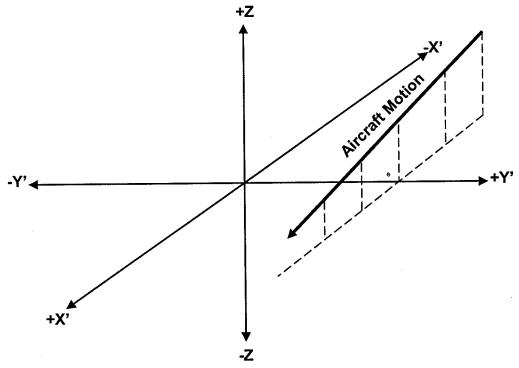

Fig. 5. Aircraft Motion in x'-y'-z space

to account for varying aircraft pitch. Consider the aircraft motion over the incremental time, dt, shown in Figure 4.

The aircraft motion depicted in Figure 4 is non-zero in both the x and y directions. The x-y plane is then rotated so that all aircraft motion in the plane occurs in the +x'-direction. The result of this rotation is shown in Figure 5.

For the aircraft to be in equilibrium in the new coordinate space, the x-z plane needs to be rotated by the pitch angle. The resulting geometry is shown in Figure 6.

Once the new coordinate systems have been established, the problem is nearly identical to the problem solved in Section III-A. The resulting free body diagram is shown in Figure 7.

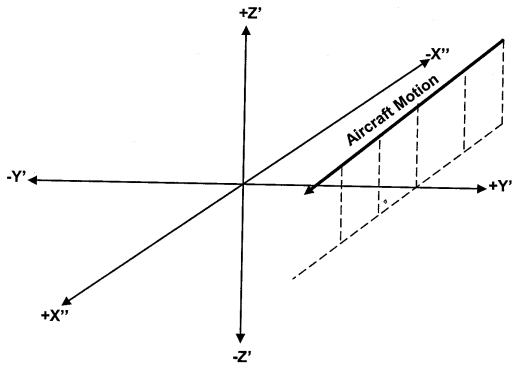

Fig. 6. Aircraft Motion in x"-y'-z' space

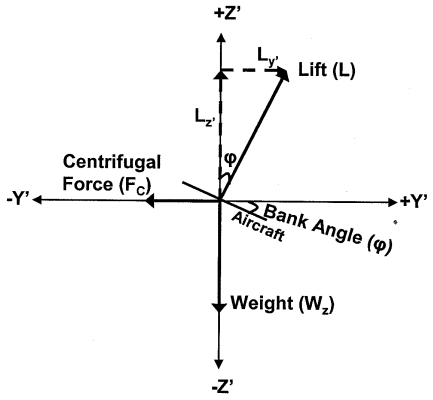

Fig. 7. Free Body Diagram of an Aircraft Executing a Varying-Altitude Banked Turn

Equations 3 through 8 are used, but require minor modifications in order to apply to the new coordinate system. Due to the rotations, the sum of forces in the y'-direction is equal to zero, meaning that

$$L_{Y'} = F_C. \tag{12}$$

Care must be taken when computing the centrifugal force in the new coordinate system. Recall that the centrifugal force is derived from Newton's Second Law. The mass term in Newton's Second Law is replaced by

$$m = \frac{W_z}{g}. \tag{13}$$

Even though the z-axis has been rotated to create the z'-axis, the weight still acts in

the direction of the -z-axis. The acceleration term in Newton's Second Law, or radial acceleration in this case, is now dependent upon the radius of curvature that exists in the x"-y' plane rather than the x-y plane. Keeping this in mind, (12) is rewritten as

$$L\sin(\phi) = \frac{W_z|v|^2}{R_{x''y'}g}, \tag{14}$$

which is solved for the roll such that

$$\phi = \arcsin\left(\frac{W_z|v|^2}{LR_{x''y'}g}\right). \tag{15}$$

Equations (6) through (8) can be applied as well, but minor changes are needed. Since the sum of forces in the z'-direction is equal to zero, it is possible to write

$$L_{z'} = W_{z'}. \tag{16}$$

Note that only the z' components of lift and weight are used in (16). Using trigonometric relations, Equation (16) is expanded to

$$L\cos(\phi) = W_z\cos(\theta). \tag{17}$$

Solving for the roll angle results in

$$\phi = \arccos\left(\frac{W_z\cos(\theta)}{L}\right). \tag{18}$$

Now (15) and (18) are combined, resulting in

$$\phi = \arctan\left(\frac{|v|^2\cos(\theta)}{R_{x''y'}g}\right). \tag{19}$$

The radius of curvature in the x"-y' plane is given by

$$R_{x''y'}(t) = \frac{[\dot{x}''(t)^2 + \dot{y}'(t)^2]^{3/2}}{\dot{x}''(t)\ddot{y}'(t) - \ddot{x}''(t)\dot{y}'(t)}. \tag{20}$$

Equation 19 provides a general equation for the roll angle that can be applied to the entire flight path. For example, when the aircraft maintains a constant altitude, θ is zero, and x" is identical to x. Under these circumstances, the radius of curvature in the x-y plane equals that in the x"-y' plane. Thus, when the aircraft maintains a constant altitude, (19) reduces to (9). Equation 19 also applies when the aircraft flies in a straight line. In such a case, the radius of curvature given by (20) approaches infinity, driving the roll angle to zero.

IV. Testing the Algorithm with Real Aircraft Flight Data

Several sample flight paths were created to test the algorithm. Four of these sample flight paths and the results of the algorithm are shown in the Appendix. A straight and level flight path is presented in Section -A of the Appendix, while a straight flight path with an increasing altitude is presented in Section -B. The remaining two sample flight paths presented in the paper contain a perfect circular flight. This maneuver is simulated first at a constant altitude, and then with a time-varying altitude, and is presented in Sections -C and -D of the Appendix, respectively.

The algorithm was then applied to data collected during F-15C Joint Helmet Cuing System mission JH-16, conducted by the 445th Flight Test Squadron at Edwards Air Force Base in May 2000. Position, pitch, and roll were recorded on board the aircraft. The aircraft heading was computed after the flight based upon the aircraft position data. The time-correlated positions were extracted from the data set to create a flight path, which serves as the input for the algorithm. The results of the algorithm were then compared to the real measured orientation angles.

A 3-D view of the F-15C flight path appears in the top panel of Figure 8, while position in the x-y plane is shown on the bottom. The x, y, and z positions are shown versus time in Figure (9). This flight path is clearly a more rigorous test of the algorithm than the sample flight paths that were simulated.

Equation 1 was used to compute the aircraft heading in the navigational coordinate system. The real and computed aircraft headings are shown in the top graph of Figure 10. The bottom graph depicts the angular difference between the real and computed heading. The computed heading matches the real heading quite well, with the mean angular error limited to 0.2 degrees, and a standard deviation of 0.1 degrees. This is to be expected, since the real heading was computed after the fact based upon the same position data used by the algorithm.

Next, the aircraft pitch was computed using (2). The top plot in Figure 11 shows the real and computed pitch, while the bottom plot shows the angular error between the two. The computed pitch shows good correlation with the pitch recorded on-board the F-15C. The mean error between the computed pitch and the real one is 3.1 degrees. The

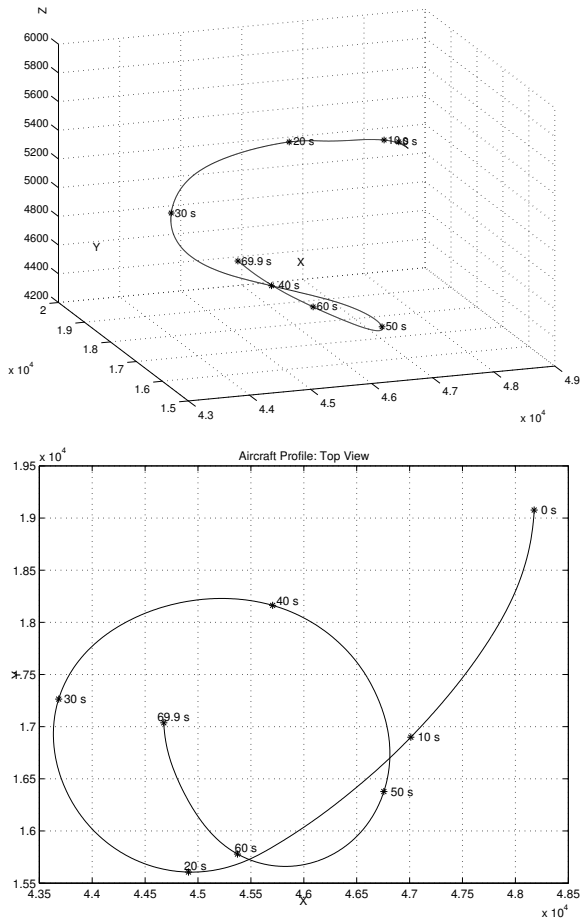

Fig. 8. 3-D (top panel) and top-down (bottom panel) views of the F-15C flight path used to test the algorithm.

standard deviation of the error is 2.3 degrees. The error in this case is probably due to the underlying assumption that the aircraft nose is pointed in the direction of the aircraft motion. The data suggests that this is a good approximation, but does not result in exact replication of the aircraft pitch.

Aircraft roll is the final parameter that is estimated by the algorithm. A comparison between the computed and real aircraft roll is shown in the top plot of Figure 12, while the bottom plot depicts the error between the two. In this case, the mean angular error between the roll computed by the algorithm and the roll recorded on-board during the flight is 2.2 degrees, with a standard deviation of 12.9 degrees. Although the mean error is not terribly large, the standard deviation reveals the difficulty of estimating aircraft roll

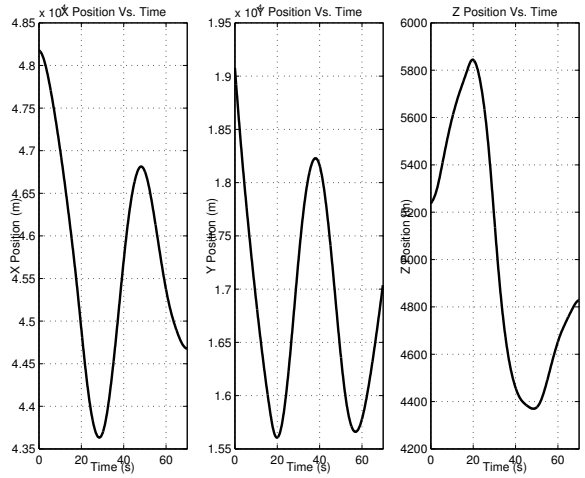

Fig. 9. X, Y, and Y positions (left to right) of the F-15C flight path used to test the algorithm.

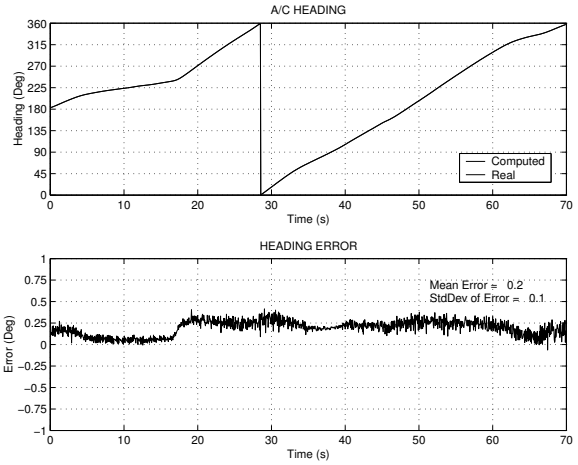

Fig. 10. Comparison of Real and Computed Aircraft Heading

from a flight path.

The difficulty in computing aircraft roll from a flight path is inherent in the problem. Modern aircraft are capable of executing roll maneuvers that do not manifest themselves in their flight paths. This renders certain determination of aircraft roll from a flight path an impossibility. The link between aircraft roll and position is simply less direct than is the case for heading and pitch. This, in turn, necessitates the need to use physics to derive aircraft roll from position; however, the derivation also induces error because it assumes that aircraft are in perfect equilibrium when executing turns. The coordinate rotations implemented in the algorithm ensure that the aircraft is in perfect vertical equilibrium.

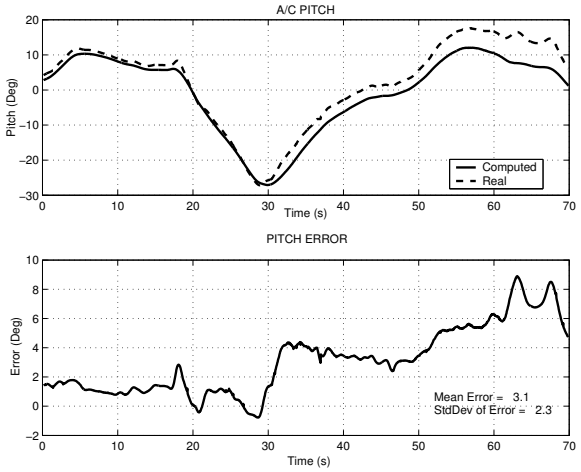

Fig. 11. Comparison of Real and Computed Aircraft Pitch

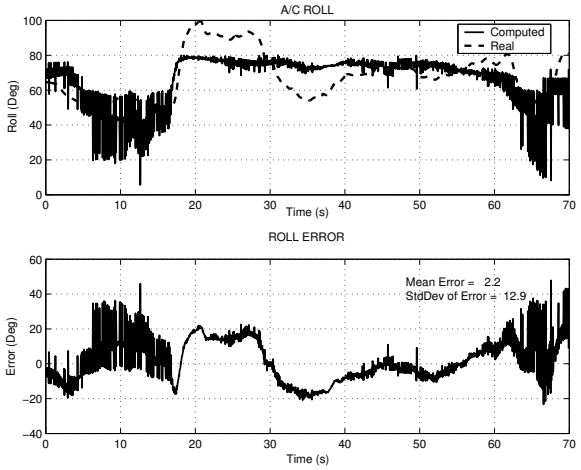

Fig. 12. Comparison of Real and Computed Aircraft Roll

Even so, nothing ensures that same is true of the horizontal plane. In reality, modern aircraft may be able to execute turns even when they are not in perfect equilibrium in the horizontal plane. The idealized derivation and lack of direct correlation between position and roll contribute to the uncertainty in the computation of aircraft roll from a flight path.

It is also noteworthy that the roll computed by the algorithm appears to be fairly noisy. This is largely due to the process used to compute the radius of curvature. The computation of the radius of curvature depends upon the first and second derivatives of position with respect to time, which must be computed from the flight path. Although the first derivatives are fairly smooth, the second derivatives that result from the process are not,

and using finite-different approximations to derivatives is numerically tricky in general. These effects are then propagated through the computations of the radius of curvature and roll. Attempts were made to filter the roll angle using an 8th order Chebyshev Type 1 low-pass filter. Although filtering did not reduce the mean error, it did make the general shape of the curve easier to discern. The filtered roll profile is shown in Figure 13.

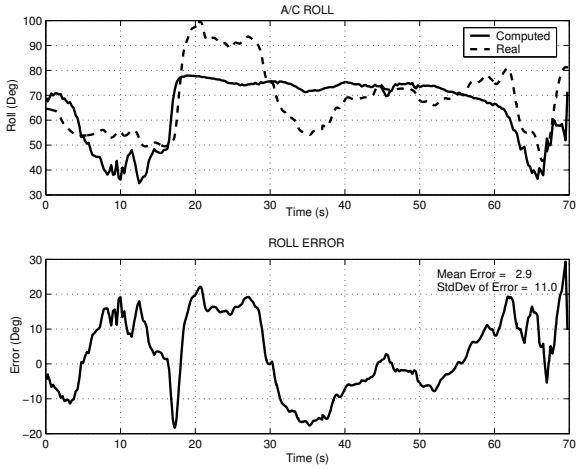

Fig. 13. Comparison of Real and Computed Aircraft Roll: Computed Roll has been Filtered

V. Conclusion

The algorithm described in this paper computes probable aircraft orientation angles, given a flight path. A certain amount of error is inherent in the process, especially in the computation of the roll angle. When this algorithm is applied to other projects, it is suggested that error bars proportional to the standard deviation of the error be placed around the computed orientation angles.

This work assumed that the positions and velocities were accurately known. In passive radar systems, velocity estimates tend to be very good due to long coherent integration times available from the continuous-wave nature of the sources, but the position errors tend to be high due to the relatively low usable bandwidth of the exploited communication signals. Future work might include an error analysis to determine how errors in the position and velocity estimates propagate through to errors in the estimates orientation estimates, which would be included in the error bars. Other effects, such as "crabbing" needed to compensate for wind speed, could also be considered.

VI. Acknowledgments

The authors would like to thank Air Force Capt. Larkin Hastriter of the University of Illinois at Urbana-Champaign and Air Force Major Adam MacDonald for their assistance in providing and interpreting the instrumented flight data.

Appendix

A. *Testing the Algorithm with a Straight-and-Level Flight Path*

The first simulated flight path used to test the algorithm is a straight-and-level flight along the +x-axis. A 3-D view is shown on the left in Figure 14, while a top view is shown on the right. Figure 15 shows the x, y, and z positions with respect to time, as well as

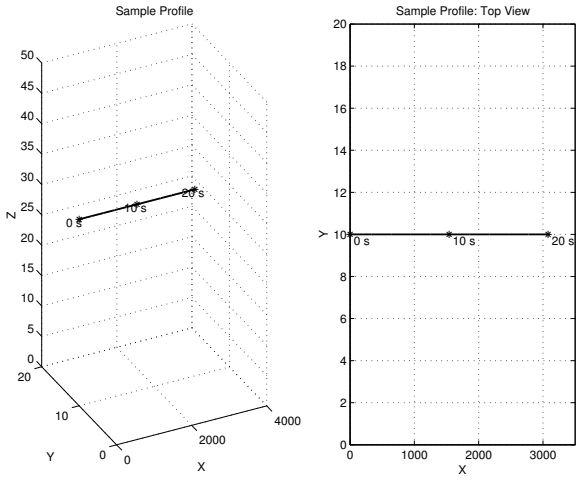

Fig. 14. Straight-and-Level Flight Profile: 3-D View and Top View (left to right)

the computed heading, pitch, and roll. The results of the algorithm in this simple case are impeccable. Since the aircraft is flying in the +x direction, the heading is 90 degrees. The aircraft pitch is zero, since the aircraft is maintaining a constant altitude. Finally, since the aircraft is not turning, the roll is zero.

B. *Testing the Algorithm with a Varying-Altitude Straight Flight Path*

The algorithm was then tested with a straight increasing-altitude flight path. This time, the aircraft was simulated flying in the -x direction. The left plot in Figure 16 shows the 3-D depiction of the simulated flight path, while the right plot shows the top view. The

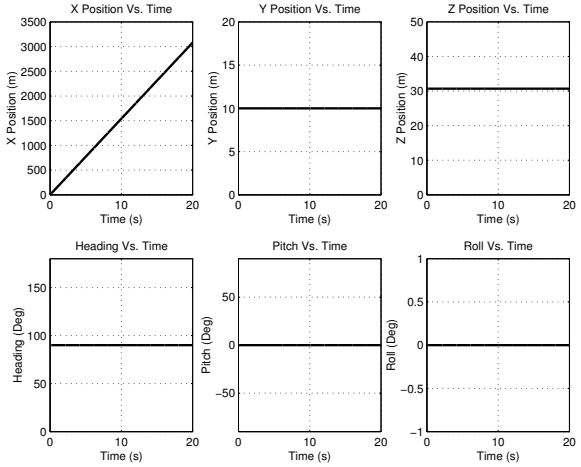

Fig. 15. Straight-and-Level Flight Profile: Positions and Computed Orientation Angles (Top Row: X, Y, Z Positions. Bottom Row: Heading, Pitch, Roll.)

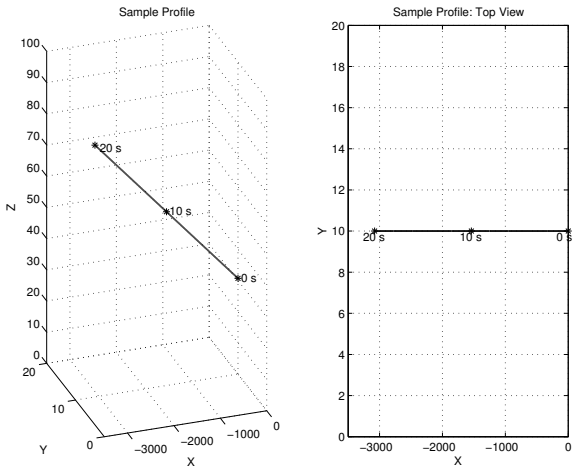

Fig. 16. Straight, Increasing-Altitude Flight Profile: 3-D View and Top View (left to right)

time-correlated positions and computed orientation angles are shown in Figure 17. Once again, the algorithm performs as expected. The heading is 270 degrees because the aircraft is flying in the -x direction. The roll is once again equal to zero, since the aircraft is not turning. The pitch is 0.93 degrees, which is consistent with the flight profile.

C. Testing the Algorithm with a Level, Circular Flight Path

A level, circular filght is the third simulated flight profile used to test the algorithm. In this case, the radius of curvature is 477.46 m, and the velocity is 150 m/s. The left plot in Figure 18 shows a 3-D view of the flight path, while the right plot shows a top view.

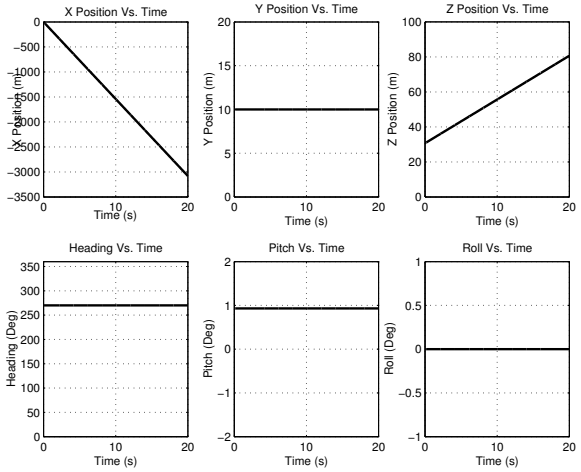

Fig. 17. Straight, Increasing-Altitude Flight Profile: Positions and Computed Orientation Angles (Top Row: X, Y, Z Positions. Bottom Row: Heading, Pitch, Roll.)

The time-correlated positions and computed orientation angles appear in Figure 19. The

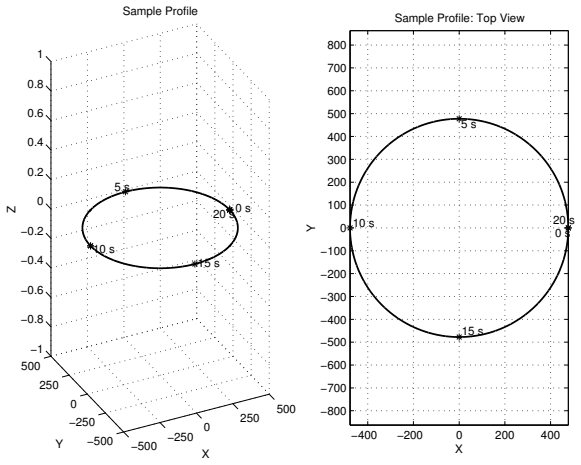

Fig. 18. Level, Circular Flight Profile: 3-D View and Top View (left to right)

aircraft heading and pitch match the expected values for the flight path. Some error is noticeable in the aircraft roll, due to the discontinuities in the computation of the radius of curvature; however, the error is minimal. Using Equation 19, the roll angle of the aircraft during the simulated maneuver is computed to be -78.24 degrees. The mean roll angle computed by the algorithm is -78.20 degrees, with a standard deviation of 0.66 degrees. This suggests that the error resulting from noise in the roll computation is minimal.

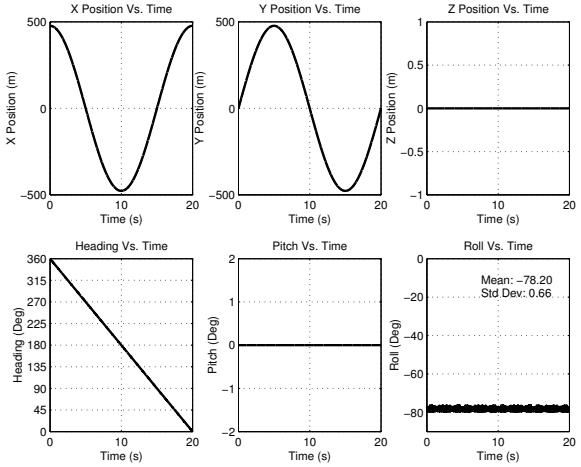

Fig. 19. Level, Circular Flight Profile: Positions and Computed Orientation Angles (Top Row: X, Y, Z Positions. Bottom Row: Heading, Pitch, Roll.)

D. Testing the Algorithm with a Varying-Altitude Circular Flight Path

The circular flight path is then repeated with an increasing altitude. The radius of curvature of the 3-D curve is 491.63 m, and the velocity is held at 150 m/s. The left plot in Figure 20 shows the 3-D view of this flight path, while the right plot shows the top view. Figure 21 shows the time-correlated positions and computed orientation angles for

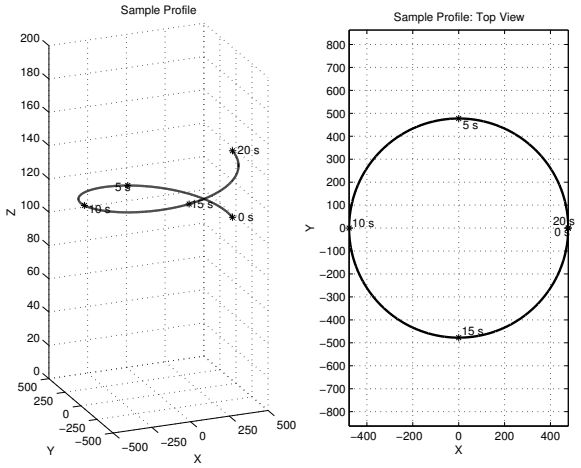

Fig. 20. Circular, Increasing-Altitude Flight Profile: 3-D View and Top View (left to right)

this simulated flight path. Once again, the heading and pitch are exactly as expected, while the roll angle computation has a small amount of error. In fact, the results are identical to those in the level-flight scenario; the algorithm computes the roll angle to be

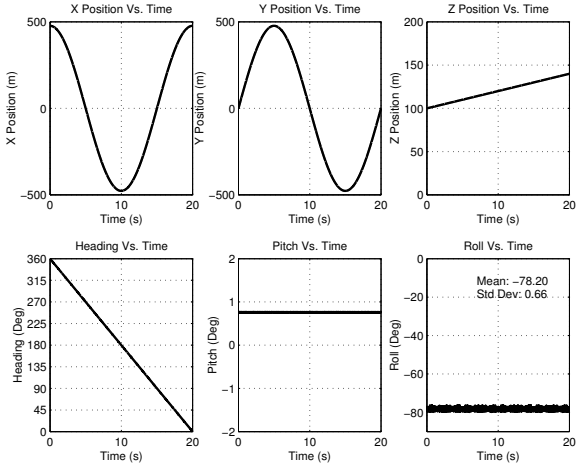

Fig. 21. Circular, Increasing-Altitude Flight Profile: Positions and Computed Orientation Angles (Top Row: X, Y, Z Positions. Bottom Row: Heading, Pitch, Roll.)

-78.20 degrees, with a standard deviation of 0.66 degrees.

References

[1] D.D. Sworder and R.G. Hutchins, "Image-enhanced tracking," *IEEE Trans. on Aerospace and Electronic Systems*, vol. 25, no. 5, pp. 701–710, Sept. 1989.

[2] D.D. Sworder and R.G. Hutchins, "Maneuver estimation using measurements of orientation," *IEEE Trans. on Aerospace and Electronic Systems*, vol. 26, no. 4, pp. 625–638, July 1990.

[3] D.D. Sworder, P.F. Singer, D. Doria, and R.G. Hutchens, "Image-enhanced estimation methods," *Proceedings of the IEEE*, vol. 81, no. 6, pp. 797–811, June 1993.

[4] D.D. Sworder, M. Kent, R. Vojak, and R.G. Hutchins, "Renewal models for maneuvering targets," *IEEE Trans. on Aerospace and Electronic Systems*, vol. 31, no. 1, pp. 138–150, Jan. 1995.

[5] J.E. Boyd and D.D. Sworder, "Tracking a maneuvering target using sensors of variable quality," *IEEE Trans. on Aerospace and Electronic Systems*, vol. 36, no. 2, pp. 501–507, April 2000.

[6] J.D. Kendrick, "Estimation of aircraft target motion using orientation measurements," *IEEE Trans. on Aerospace and Electronic Systems*, vol. 17, no. 2, pp. 254–259, Mar. 1981.

[7] C.C. Lefas, "Algorithms for improved, heading assisted, maneuver tracking," *IEEE Trans. on Aerospace and Electronic Systems*, vol. 21, no. 3, pp. 351–359, May 1985.

[8] M.I. Miller, A. Srivastava, and U. Grenander, "Conditional-mean estimation via jump-diffusion processes in multiple target tracking/recognition," *IEEE Trans. on Signal Processing*, vol. 43, no. 11, pp. 2678–2690, November 1995.

[9] U. Grenander and M. I. Miller, "Representations of knowledge in complex systems," *Journal of the Royal Statistical Society B*, vol. 56, no. 3, pp. 549–603, 1994.

[10] A. Srivastava, U. Grenander, G. Jensen, and M.I. Miller, "Inferences via jump-diffusion processes on matrix Lie groups," *Submitted to Advances in Applied Probability*, August 1996.

[11] A. Srivastava, *Inference on Transformation Groups Generating Patterns on Rigid Motions*, D.Sc. Dissertation, Dept. of Electrical Engineering, Sever Institute of Technology, Washington Univ., St. Louis, MO, August 1996.

[12] S.C. Herman and P. Moulin, "A particle filtering approach to joint radar tracking and automatic target recognition," in *Proc. IEEE Aerospace Conference*, Big Sky, Montana, March 10-15 2002.

[13] S.M. Herman, *A Particle Filtering Approach to Joint Passive Radar Tracking and Target Classification*, Doctoral Dissertation, Department of Electrical and Computer Engineering, Univ. of Illinois at Urbana-Champaign, Urbana, IL, 2002.

[14] P.E. Howland, *Television Based Bistatic Radar*, Ph.D. thesis, University of Birmingham, England, 1997.

[15] C.E. Dole, *Flight Theory and Aerodynamics*, John Wiley & Sons, 1981.

[16] A.M. Kuethe and C.-Y. Chow, *Foundations of Aerodynamcis: Bases of Aerodynamic Design, 3rd Edition*, John Wiley & Sons, 1976.

[17] C.F. Meyer and D.W. Gibson, *Route Surveying and Design, 5th Edition*, Harper & Row, Publishers, 1980.